國立交通大學

電機與控制工程學系

博 士 論 文

低功率影像處理電路於腸胃道內視鏡之研究

Study on Low-Power Image Processing Circuits for Gastrointestinal Endoscopy

研 究 生：林盟淳

指導教授：董蘭榮 教授

中 華 民 國 九 十 六 年 十 月

低功率影像處理電路於腸胃道內視鏡之研究

Study on Low-Power Image Processing Circuits for Gastrointestinal Endoscopy
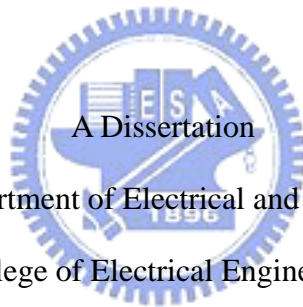
研 究 生：林盟淳　　　　　　Student：Meng-Chun Lin

指導教授：董蘭榮　　　　　　Advisor：Lan-Rong Dung

國 立 交 通 大 學

電 機 與 控 制 工 程 學 系

博 士 論 文

A Dissertation

Submitted to Department of Electrical and Control Engineering

College of Electrical Engineering

National Chiao Tung University

in partial Fulfillment of the Requirements

for the Degree of

Doctor of Philosophy

in

Electrical and Control Engineering

October 2007

Hsinchu, Taiwan, Republic of China

中 華 民 國 九 十 六 年 十 月

低功率影像處理電路於腸胃道內視鏡之研究

研究生：林盟淳　　　　　　　　　　指導教授：董蘭榮 博士

國立交通大學電機與控制工程學系(研究所)博士班

摘要

對於無線腸胃道內視鏡系統，我們已經成功發展出兩種應用於膠囊內視鏡或是吞嚥式影像膠囊的極低功率影像壓縮處理器。在無線膠囊內視鏡系統應用中，平衡壓縮端電池壽命/效能取捨是極為重要的。取代目前最先進的影像壓縮技術，我們首先提出一套以紅綠藍三原色為基礎的影像壓縮演算法，簡稱為 GICam-I 且此演算法首先藉由移除傳統影像壓縮演算法內的解碼賽克(demosaicking)技術與色彩空間轉換(color-space transform)技術來簡化傳統影像壓縮演算法的計算複雜度。另外，為了更進一步延長無線腸胃道內視鏡系統壓縮端的電池使用壽命，我們接著發展出一套改良式、極低功率、以次取樣(subsample)技術為基礎的影像壓縮演算法，簡稱為 GICam-II。藉由次取樣技術來改良 GICam-I 演算法的計算負載，根據色彩敏感度分析的結果，我們成功利用次取樣技術去降低綠色訊號與藍色訊號的記憶體需求。

除了使用極低功率壓縮技術來節省在高解析度無線腸胃道內視鏡系統的射頻傳輸功率損耗。對於無線/有線腸胃道內視鏡系統，如何有效消除惱人的脈衝雜訊與強化腸胃道影像的銳利度是必然。為了克服這些問題，低-高-中(lower-upper-middle, LUM)濾波器是最適當的候選因為它本身同時具有平滑化與銳利化的能力。在 LUM 濾波器的運算中，主要運算核心為排序濾波器(rank-order filtering, ROF)計算且 LUM 濾波器需要不同的順序(rank)值來完成平滑化或是銳利化的任務。因此需要一個有彈性的 ROF 硬體來供任意選擇所需要的順序值已完成 LUM 濾波器的運算程序且我們已經提出一個以可遮罩式記憶體為基礎的排序濾波器架構。可遮罩式記憶體結構又稱為雙細胞隨機存取記憶體(dual-cell random-access memory, DCRAM)是一個伴隨著可遮罩式暫存器與雙細胞結構的靜態隨機存取記憶體(static random-access memory, SRAM)的延伸變化。本論文是第一個使用可遮罩式記憶體來實現排序濾波器，藉由一般排序濾波器演算法驅動，以此記憶體為基礎的硬體架構具有高彈性與高規則性且同時擁有低成本與高效能之特色。這個架構能夠應用於任意順序的尋找以及包含遞歸(recursive)或是非遞歸(non-recursive)的排序濾波器之變形。除了針對腸胃道影像可以消除惱人的脈衝雜訊及增加其影像銳利度外，本論文所提出的排序濾波器之運算速度也可以應付即時影像處理應用。

Study on Low-Power Image Processing for Gastrointestinal Endoscopy

Student: Meng-Chun Lin   Advisor: Lan-Rong Dung

Department of Electrical and Control Engineering

National Chiao-Tung University

Abstract

For wireless gastrointestinal endoscope systems, we have successfully developed two kinds of ultra-low-power image compression processors applied for capsule endoscope or swallowable imaging capsules. In applications of wireless endoscope systems, it is imperative to balance battery life/performance trade-offs. Instead of applying state-of-the-art image compression techniques, we first proposed an RGB-based compression algorithm, called GICam-I and it firstly simplified traditional image compression algorithms by removing the demosaicking technique and the color-space transformation. In addition, to further extend the battery life in wireless gastrointestinal endoscope systems, another improved ultra-low-power subsample-based GICam image compression processor, called GICam-II, is proposed. By using the subsample technique to improve computational loads in the GICam-I, we successfully make use of the subsample technique to reduce the memory requirements of G1, G2 and B components according to the analysis results of color sensitivity.

Except using novel ultra-low-power compression techniques to save the power dissipation of RF transmitter in high-resolution wireless gastrointestinal endoscope systems. How to efficiently eliminate annoying impulsive noise caused by a fault sensor and enhance the sharpness is necessary for gastrointestinal (GI) images in wired/wireless gastrointestinal endoscope systems. To overcome these problems, the LUM filter is the most suitable candidate because it simultaneously has the characteristics of smoothing and sharpening. In the operational procedure of LUM filter, the mainly operational core is the rank-order filtering (ROF) and the LUM filter itself needs to use different kind of rank values to accomplish the task of smoothing or sharpening. Therefore, we need a flexible ROF hardware

to arbitrarily select wanted rank values into the operation procedure of LUM filter and we have proposed an architecture based on a maskable memory for rank-order filtering. The maskable memory structure, called dual-cell random-access memory (DCRAM), is an extended SRAM structure with maskable registers and dual cells. This dissertation is the first literature using maskable memory to realize ROF. Driving by the generic rank-order filtering algorithm, the memory-based architecture features high degree of flexibility and regularity while the cost is low and the performance is high. This architecture can be applied for arbitrary ranks and a variety of ROF applications, including recursive and non-recursive algorithms. Except efficiently eliminating annoying impulsive noises and enhance sharpness for GI images, the processing speed of ROF can also meet the real-time image applications.

致 謝

對於本論文的完成，首先要感謝的是我的指導教授 董蘭榮教授，感謝老師在我的碩士班與博士班這六年來，給予我相當多珍貴的意見與指導，往往能夠讓我茅塞頓開，並且能從許多層面去思考問題。這段時間也從老師身上學到了許多研究的態度與寶貴的知識，讓我能夠用更成熟與積極的態度來面對自己的研究。此外，也很謝謝老師給予我機會去參與許多比賽與研究計畫，讓我能夠有機會獲得更多的磨鍊。

感謝論文口試委員吳重雨校長、林進燈教務長、劉正典教授與鄺獻榮教授的指導，對這篇論文提出批評指教，使得本論文可以更加完善。此外，要感謝實驗室的同學與學弟巫穎毅、黃建發、陳育聖，業松樹、陳泰佑、宋岳璋、賴信丞、林炫伯與邱致翰等在這四年的研究生活上的幫助。以及台北醫學大學附設醫院潘憲前院長、劉正典前副院長與張君照主任在臨床應用上的寶貴意見與指導。另外，也要感謝我的室友陳益生與蘇宗敏，從你們那邊我學到了許多關於論文投稿的知識與未來生涯規劃的想法。

最後，要感謝我的父母、哥哥盟翔、大嫂薈茹以及我的太太珮雯及其家人，讓我沒有後顧之憂，沒有你們的支持，我亦無法順利畢業。

Contents

vii

List of Figures

List of Tables

1

Introduction

1.1 Research Objective

During the past decades, diseases of the gastrointestinal (GI) tract, such as stomach and colon cancers, are common in most countries. Most GI cancers can be remedied if they are diagnosed at their early phase. Current GI endoscopes can be categorized into two major groups: wired active endoscope systems and wireless passive endoscope systems. Much works have been studied in the wired active endoscope systems [1, 2, 3, 4, 5, 6]. Modem fiber-optic based endoscopy made visualization of the whole stomach, upper small intestine and colon possible. The procedures used to examine them, namely gastroscopy, small-intestine endoscopy and colonoscopy cause discomfort and pain to the patients because they require flexible, relatively bulky cables to be pushed into the intestine. These cables are necessary to carry light by fiber-optic bundles, provide power and transmit video signals. Small-intestine endoscopy in particular is severely constrained by problems of discomfort and limitations of how far enteroscopes can be advanced into the small-intestine. Small-bowel endoscopy in particular is constrained by problems of discomfort and limitations of how far they can he advanced into the small bowel. There is a clinical need for improved methods of examining the small bowel and colon, especially in patients with GI bleeding. Despite all the drawbacks, wired active GI endoscopy is still the most effective and widely used diagnostic procedure in detecting diseases of the GI tract. Therefore, in order to

support the best diagnosis results in clinics, the image enhance plays the most important key component in wired active endoscope systems.

Although the wired active endoscope systems can enable efficient diagnosis based on real images and biopsy samples, it causes patients discomfort and pain to push flexible, relatively bulky cables into the digestive tube. To relief the suffering of patients, wireless passive endoscope systems are being developed worldwide [7, 8, 9, 10, 11, 12, 13]. However, based on clinical experience; the wireless passive endoscope system still have some drawbacks. First, the wireless passive endoscope system cannot control its heading and moving direction itself. This drawback may cause image oversights and miss a disease. Second, the resolution of demosaicked image is still low, and some interesting spots may be unintentionally omitted. The first drawback is the nature of passive endoscopy. Some papers have presented approaches for the autonomous moving function [14, 15, 16, 17]. Very few papers address the solutions of the second drawback. Increasing resolution may alleviate the second problem; however, it would result in significant power consumption in RF transmitter. Hence, applying a image compression technique is necessary for saving the power dissipation of RF transmitter. Except low resolution problem in the current wireless passive endoscope systems, the image enhancement also plays another important issue because the interference of impulsive noise caused by a faulty sensor during image acquisition and the visual-quality degradation during the lossy image compression processing for decoded GI images. the former can efficiently use the noise reduction technique to suppress the impulsive noise and the later can also use the sharpening technique to enhance the edge gradient of a decoded GI image validly.

Therefore, this dissertation mainly focuses on two goals, The first goal is to solve the second drawback of the wireless passive capsule endoscope systems, namely the low resolution for demosaicked GI images. The second goal is to accomplish tasks of image enhancement using a highly flexible and configurable image processor that has abilities of noise suppression and sharpness simultaneously and can deal with a full region or particular region in a GI image.

1.2 Organization of the Dissertation

The dissertation is organized as follows. In Chapter 2, the wired active endoscopes and the wireless passive capsule endoscope systems will be introduced in detail. In Chapter 3, two kinds of ultra-low-power image compression processors are proposed for capsule endoscope or swallowable imaging capsules. In applications of capsule endoscopy, it is imperative to consider battery life/performance trade-offs. Instead of applying state-of-the-art video compression techniques, Section 3.1 proposes an RGB-based compression algorithm, called GICam-I. In which the memory size and computational load can be significantly reduced. this algorithm first simplified traditional video compression algorithms by removing the demosaicking technique and the color-space transformation. In addition, to further extend the battery life of capsule endoscope, Section 3.2 quantitatively analyzes the importance of each primary colors respectively and defines the desired subsample ratios to red, green and blue signals in a GI image. According to the analysis of color sensitivity in Section 3.2, Section 3.3 proposes a subsample-based GICam image compressor, called GICam-II. This GICam-II algorithm firstly make use of the subsample technique to further reduce the memory requirements in the coding process.

Chapter 4 proposes an architecture based on a maskable memory for rank-order filtering. This dissertation is the first literature using maskable memory to realize the mainly operational core of lower-upper-middle (LUM) filtering processor; rank-order filtering (ROF). Driving by the generic rank-order filtering algorithm, the memory-based architecture features high degree of flexibility and regularity while the cost is low and the performance is high. With the LIW instruction set, this architecture can be applied for arbitrary ranks and a variety of ROF applications, including recursive and non-recursive algorithms. As shown in the implementation results, the core of the processor has high performance and low cost. The post-layout simulation shows that the power consumption can be as low as 7 mW at 256 MHz. Except efficiently eliminate annoying impulsive noises and spot-points caused by a sensor for a noisy GI image, the processing speed can also meet the real-time requirement of image applications in the QCIF, CIF, VGA, or SVGA formats. Finally, Chapter 5 concludes this dissertation and discusses the related future research.

2

Study on Wired/Wireless Gastrointestinal Endoscope Systems

During the past decades, diseases of the gastrointestinal (GI) tract, such as stomach and colon cancers, are common in most countries. Most GI cancers can be remedied if they are diagnosed at their early phase. There are several methods to detect GI diseases without adopting intrusive devices into the human body. However, the conventional GI endoscopy is irreplaceable because it enables diagnosis based on analysis of real images and biopsy samples. Many research institutions and industries have embarked on the effort to improve conventional GI endoscopy procedures. Current GI endoscopes can be categorized into two major groups: wired active endoscope systems and wireless passive endoscope systems.

In Chapter 2, the wired active endoscopes and the wireless passive endoscopes will be introduced in detail. Through the study in Section 2.1, operations of the wired active gastrointestinal(GI) endoscopes will be completely exposed and we can also understand the advantage and disadvantage obviously for the wired active gastrointestinal(GI) endoscopy. As the same as Section 2.1, Section 2.2 also do the same thing for wireless passive gastrointestinal(GI) endoscopes. Finally, we will clearly indicate problems that should be solved at the end of chapter 2.

2.1 Study on A Wired Active Gastrointestinal Endoscope System

Fig.2.1 illustrates a wired active gastrointestinal endoscope system and the color image sensor (**CIS**) firstly senses primary colors of each pixels through the color filtering array. The color filtering array can filter three color arrays that include primary colors for a GI image. Next, a GI image generated by the **CIS** can pass through the red route and then is showed on the monitor of Display. A professional doctor can execute the clinic according to the current GI image shown on the monitor. If the visual quality of current GI image is good and there is no interference occurs, the current GI image can be stored through the control of the **Photography Requesting**. On the contrary, if the doctor want to diagnose the syndrome in detail, the **Syndrome Recognition** will announce information to the **Photography Requesting** and then the **Photography Requesting** will control the **Image Enhancement** to accomplish the task of syndrome enhancement. The **Image Enhancement** can mainly accomplish three kinds of tasks. The first task is the image smoothing, the second task is the edge enhancement and the third task is the syndrome enhancement. The image smoothing mainly eliminates the annoying impulsive noises caused by the fault sensor. The edge enhancement should efficiently enhance the sharpness of a GI image and the syndrome enhancement can enhance the syndrome characteristics that doctors want to diagnose. These tasks all can process in full of regions or a particular region for a GI image. Due to the data domain in the **Image Enhancement** is the type of YCbCr, hence the **Color Transform** transfers RGB colors into YCbCr values before starting the **Image Enhancement**. Finally, the **Color Transform** will transfer YCbCr values of results into RGB colors again before displaying on the monitor of **Display**.

Much works have been studied in the wired active endoscope systems [1, 2, 3, 4, 5, 6]. Modem fiber-optic based endoscopy made visualization of the whole stomach, upper small intestine and colon possible. The procedures used to examine them, namely gastroscopy, small-intestine endoscopy and colonoscopy cause discomfort and pain to the patients because they require flexible, relatively bulky cables to be pushed into the intestine. These cables are necessary to carry light by fiber-optic bundles, provide power and transmit video
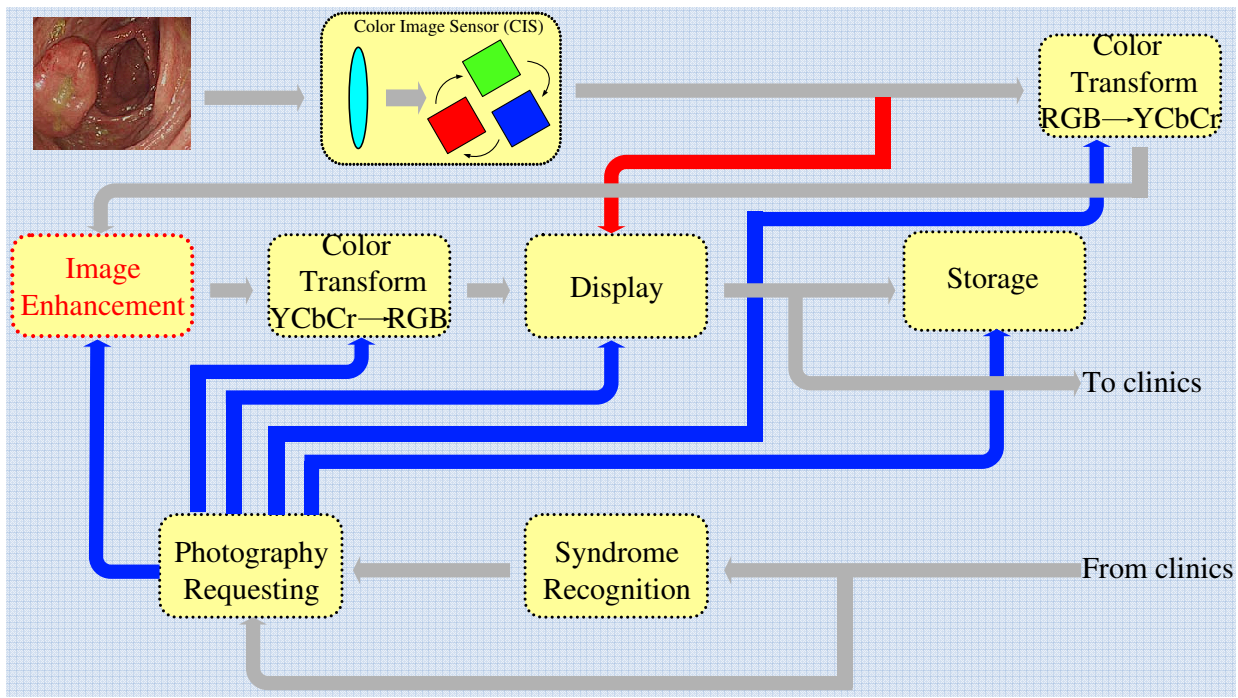
Figure 2.1. A wired active gastrointestinal endoscope system.

signals. Small-intestine endoscopy in particular is severely constrained by problems of discomfort and limitations of how far enteroscopes can be advanced into the small-intestine. Small-bowel endoscopy in particular is constrained by problems of discomfort and limitations of how far they can he advanced into the small bowel. There is a clinical need for improved methods of examining the small bowel and colon, especially in patients with GI bleeding. Despite all the drawbacks, wired active GI endoscopy is still the most effective and widely used diagnostic procedure in detecting diseases of the GI tract. Therefore, in order to support the best diagnosis results in a clinic, the **Image Enhancement** plays the most important role in wired active endoscope systems.

2.2 Study on A Wireless Passive Gastrointestinal Endoscope System

Although the wired active endoscope systems can enable efficient diagnosis based on real images and biopsy samples, it causes patients discomfort and pain to push flexible, relatively

bulky cables into the digestive tube. To relief the suffering of patients, wireless passive endoscope systems are being developed worldwide [7, 8, 9, 10, 11, 12, 13]. In the category of wireless passive capsule endoscopes, the state-of-the-art is represented by a commercial wireless capsule endoscope product, the Pillcam (with the previous model named M2A) capsule [7, 8, 12] developed by an Israeli company, Given Imaging Ltd. The Pillcam capsule is equipped with a tiny CMOS camera, a wireless transmitter to send out the images, and a battery cell to power the device. The Pillcam capsule can be swallowed through the patient's mouth and it then moves completely passive with the natural peristaltic movement of the human GI system. Similar designs of wireless passive capsule endoscopes to the Pillcam capsule were reported by paper [10, 11]. Except the Pillcam, FS System Lab Company of Japan is developing its own super-micro capsule endoscope code named Norika [13]. The Norika3 is externally powered and can be controlled via external magnetic field to move and rotate.

From these state-of-the-art products, the most popular wireless capsule endoscope product is still the Pillcam capsule. The Pillcam capsule mainly transmits the GI images at the resolution of 256-by-256 8-bit pixels and the frame rate of 2 frames/sec (or fps). Because of its high mobility, it has been successfully utilized to diagnose diseases of the small intestine and alleviate the discomfort and pain of patients. However, based on clinical experience; the Pillcam still has some drawbacks. First, the Pillcam cannot control its heading and moving direction itself and it needs 8 to 24 hours or more to go through the procedure. Since the movement of the capsule is not controlled, missing diagnosis is possible. This drawback may cause image oversights and miss a disease. Second, the resolution of demosaicked image is still low, and some interesting spots may be unintentionally omitted. Especially, the images will be severely distorted when physicians zoom images in for detailed diagnosis. The first drawback is the nature of passive endoscopy. Some papers have presented approaches for the autonomous moving function [14, 15, 16, 17]. Paper [15] proposed a magnetic actuator for use in a capsule endoscope. This is the first time that an external actuation mechanism for actively driving a wireless capsule endoscope is reported and the experimental studies on a dummy capsule were carried out. It uses a permanent magnet inside the capsule and an external rotational magnetic field to rotate the capsule. With the help of a 1mm high spiral structure on the outer surface of the capsule, the rotational movement of the capsule

by the external rotational magnetic field transfers to forward movement of the capsule. The experimental study was performed on a dummy capsule structure without any endoscope functions.

Very few papers address the solutions of the second drawback. Increasing resolution may alleviate the second problem; however, it would result in significant power consumption in RF transmitter. Hence, applying a image compression technique is necessary for saving the power dissipation of RF transmitter [18, 19]. Although papers [18, 19] can efficiently propose modified image coding algorithms in applications of wireless GI capsule endoscopy, these image compression algorithms still dissipate redundant computational-power because they all require two preprocessing steps that are demosaicking and the color space transformation before starting the coding process. The demosaicking step requires weighted sums for color interpolation and the color space transformation requires calculation of inner products. From the view point of low-power image coding in applications of wireless GI capsule endoscopy, it is not worth it to dissipate power for both preprocessing steps as long as the compression quality and ratio are acceptable.

To both overcome the second drawback and balance battery life/performance trade-offs, Fig.2.2 illustrates the wireless passive endoscope system and this system consists of two parts, one is encoder and the other is decoder. In the encoder stage, the color image sensor **(CIS)** firstly senses a 512×512 color GI image as the Bayer format while color filtering uses Bayer patterns. Due to save the power dissipation of RF transmitter and keep the current frame rate of 2 frames/sec (or fps) in the modern specification of these state-of-the-art products, the compression ratio should be above 4-to-1 in the **Image Coding**. After finishing the **Image Coding**, the **Channel Coding** encrypts the encoded bit streams to avoid data loss in the channel of RF transmitting. In the decoder stage, the RF Receiver receives the encryption datum and then the **Channel Decoding** restores the encryption datum while the datum suffer distortion. The **Image Decoding** decodes the output datum from the **Channel Decoding** and the decoded Bayer format is lossy because the **Image Coding** and **Image Decoding** both belong to the lossy image compression procedure. After accomplishing the task of **Image Decoding**, the **Demosaicking** uses weighted sum for color interpolation and generates a demosaicked GI image. Next, a demosaicked GI

8

image generated by the **CIS** can pass through the red route and then is showed on the monitor of Display. A professional doctor can execute the clinic according to the current GI image shown on the monitor. If the visual quality of current GI image is good and there is no interference occurs, the current GI image can be stored through the control of the **Photography Requesting**. On the contrary, if the doctor want to diagnose the syndrome in detail, the **Syndrome Recognition** will announce information to the **Photography Requesting** and then the **Photography Requesting** will control the **Image Enhancement** to accomplish the task of syndrome enhancement. The **Image Enhancement** can mainly accomplish three kinds of tasks. The first task is the image smoothing, the second task is the edge enhancement and the third task is the syndrome enhancement. The image smoothing mainly eliminates the annoying impulsive noises caused by the fault sensor. The edge enhancement should efficiently enhance the sharpness of a GI image because the visual-quality degradation during the lossy image compression processing and the syndrome enhancement can enhance the syndrome characteristics that doctors want to diagnose. These tasks all can process in full of regions or a particular region for a GI image. Due to the data domain in the **Image Enhancement** is the type of YCbCr, hence the **Color Transform** transfers RGB colors into YCbCr values before starting the **Image Enhancement**. Finally, the **Color Transform** will transfer YCbCr values of results into RGB colors again before displaying on the monitor of **Display**.

Chapter 3 will propose two kinds of ultra-lower-power image coding algorithm to solve the problem of low resolution for wireless GI capsule endoscopy systems in detail and Chapter 4 will propose a highly flexible and configurable non-linear filtering hardware to accomplish the task of image enhance according to demands of users for wired active endoscope systems and wireless passive endoscope systems.
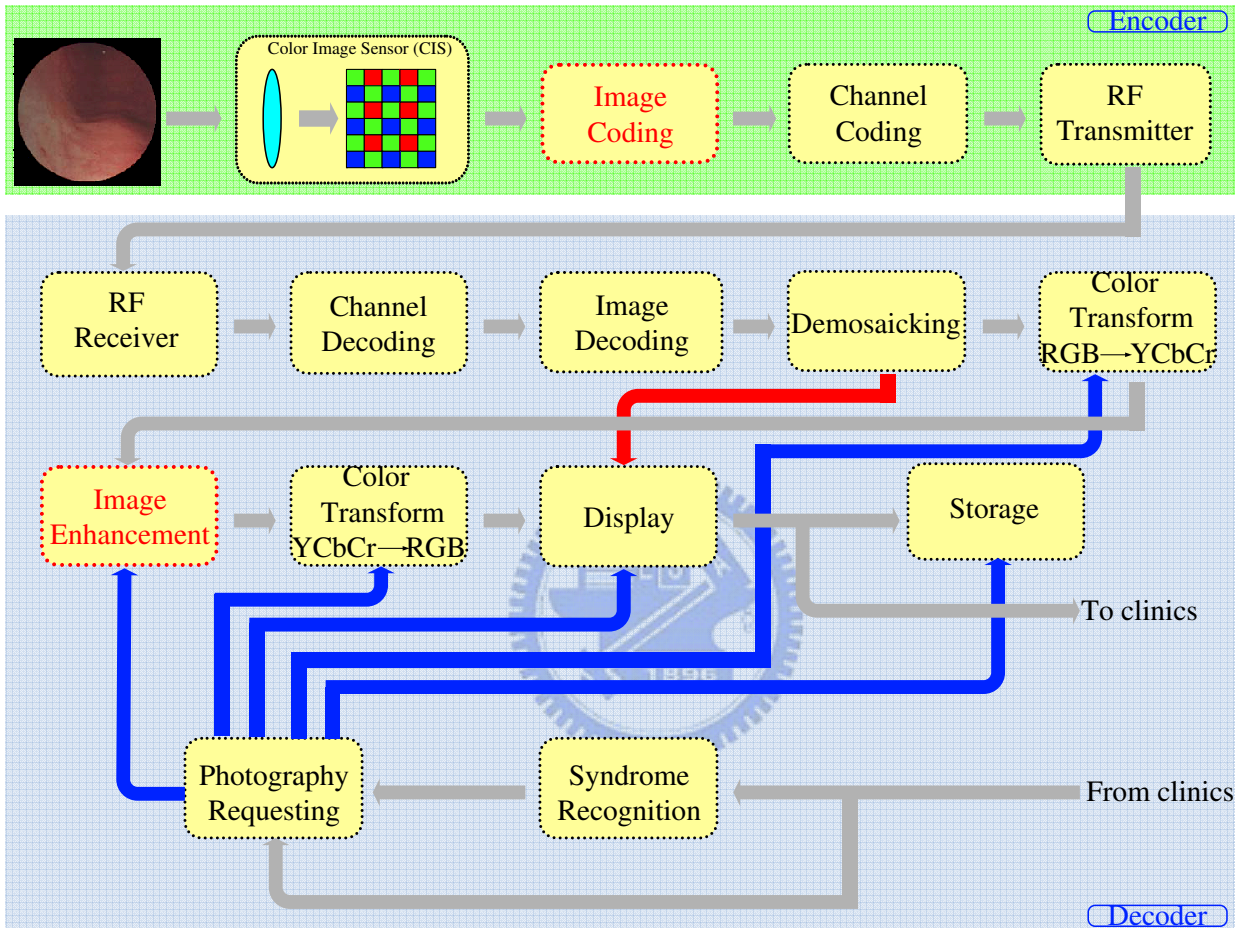
Figure 2.2. A wireless passive gastrointestinal endoscope system.

3

Encoder for Wireless Gastrointestinal Endoscopy

In this chapter, two kinds of ultra-low-power image compression processors are proposed for capsule endoscope or swallowable imaging capsules. In applications of capsule endoscopy, it is imperative to consider battery life/performance trade-offs. Instead of applying state-of-the-art video compression techniques, we first propose an RGB-based compression algorithm, called GICam-I. In which the memory size and computational load can be significantly reduced. We first simplified traditional image compression algorithms by removing the demosaicking technique and the color-space transformation. In addition, to further extend the battery life of capsule endoscope, we herein present a subsample-based GICam image compressor, called GICam-II. The GICam-II firstly make use of the subsample technique to further reduce the memory requirements of G1, G2 and B components in the coding process according to the analysis results of color sensitivity.

3.1 The RGB-based GICam Image Compression Algorithm (GICam-I)

Fig.3.1 illustrates the system diagram of the proposed capsule endoscope. We attached an ultra-low-power image compressor to the CMOS sensor to deliver a compressed 512×512 image. The compression ratio is above 4-to-1 such that the frame rate can be 2 frames per second (fps) when the wireless transmission rate is at 0.5 megabits per second. To reduce the buffer size between the CMOS sensor and the image compressor, the scanline controller is dedicated to scan out R, G1, G2, and B signals in a certain order.

Traditional image compression algorithms use the optimized quantization for YCbCr image to reduce compressed image size while the visual distortion is low. In order to quantize YCbCr image, the typical image compression requires two preprocessing steps that are demosaicking and the color space transformation. However, the demosaicking step requires weighted sums for color interpolation and the color space transformation requires calculation of inner products. From the view point of GICam, it is not worth it to dissipate power for both preprocessing steps as long as the compression quality and ratio are acceptable. Hence, Fig.3.2 illustrates the power saving on the GICam image compressor, called GICam-I. First of all, the GICam-I directly processes raw images without demosaicking and color space transform. For a 512×512 image, when using the Bayer format, the image has 512×512 Bayer patterns. Fig.3.3 shows the Bayer patterns in the CMOS image sensor. So, the incoming image size to the 2D-DCT is 256×256×8×4 bits, where each pixel is an 8-bit datum and each of R, G1, G2, and B components has 256×256 pixels. Since the image size after preprocessing in the traditional algorithm is 512×512×8×3 bits, the computational load of 2D-DCT and quantization is reduced by the factor of 3.

Traditional compression algorithms employ the YCbCr quantization to earn a good compression ratio while the visual distortion is minimized, based on the factors related to the sensitivity of the human visual system (HVS). However, for the sake of power saving, our compression rather uses the RGB quantization [21] to save the computation of demosaicking and color space transformation. As mentioned above, the advantage of applying RGB
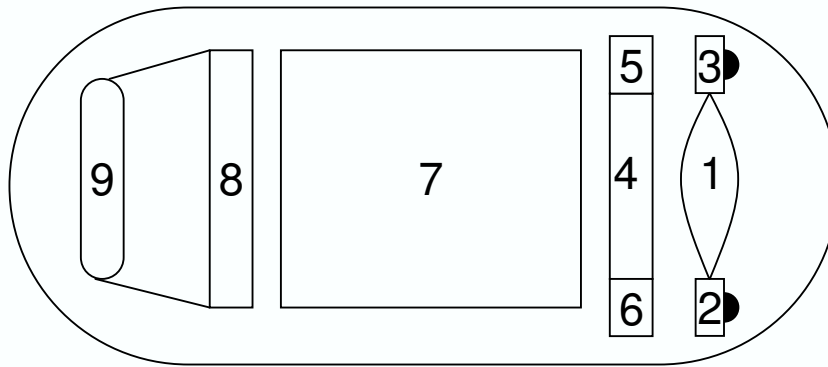
Figure 3.1. The system structure of GICam. (1: Len; 2,3: LEDs; 4: CMOS sensor; 5: Image compressor; 6: Scanline controller; 7: Battery; 8: RF transmitter; 9: Antenna.

quantization is two-fold: saving the power dissipation on preprocessing steps and reducing the computing load of 2D-DCT and quantization. Moreover, to reduce the hardware cost and quantization power dissipation, we modified the RGB quantization tables in [21] as shown in Fig.3.4 and the quantization multipliers are power-of two's. In GICam-I, the Lempel-Ziv (LZ) coding [24] is employed for the entropy coding. The reason why we adopted the LZ coding as the entropy coding is that the LZ encoding does not need look-up tables and complex computation. Thus, the LZ encoding can consume less power and use smaller silicon size than the other candidates, such as the Huffman encoding and the arithmetic coding. The target compression performance of the GICam-I is to reduce image size by 75% at least. To meet the specification, given the quantization tables, we exploited the cost-optimal LZ coding parameters. There are two parameters in the LZ coding to be determined; they are the window size, w, and the maximum matching length, l. As seen in Fig.3.5, simulating with twelve endoscopic pictures shown in Fig.3.7, (64, 16) is the minimum (w, l) set to meet the compression ratio requirement by simulating with 12 endoscopic pictures.

When comparing the proposed image compression with the traditional one in paper [20], the power dissipation of GICam-I can save 98.2% because of the reduction of memory requirement. However, extending the utilization of battery life for a capsule endoscope is still an very important issue. According to the power analysis generated by PrimePower^{TM}, the total power dissipation of GICam-I is 14.92 mW while operating at 1.8 V, in which, the power consumption of logic part is 5.52 mW, and the memory blocks generated by Artisan
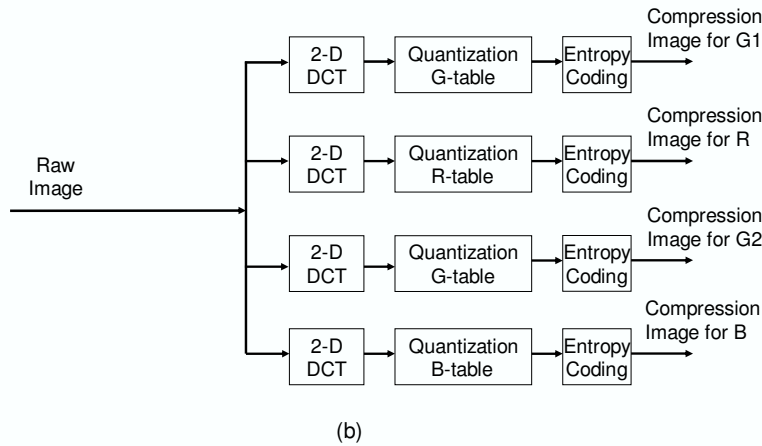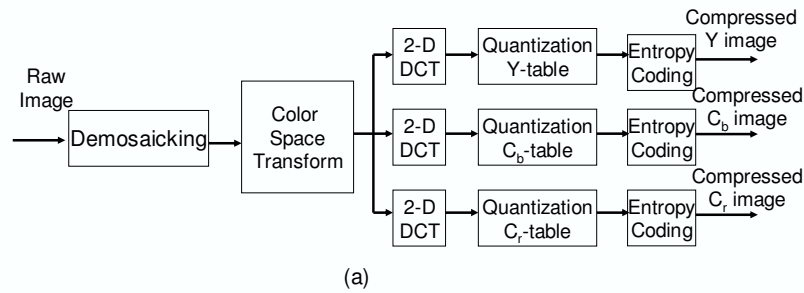
Figure 3.2. (a) A typical image compression algorithm. (b) The GICam-I image compression algorithm.
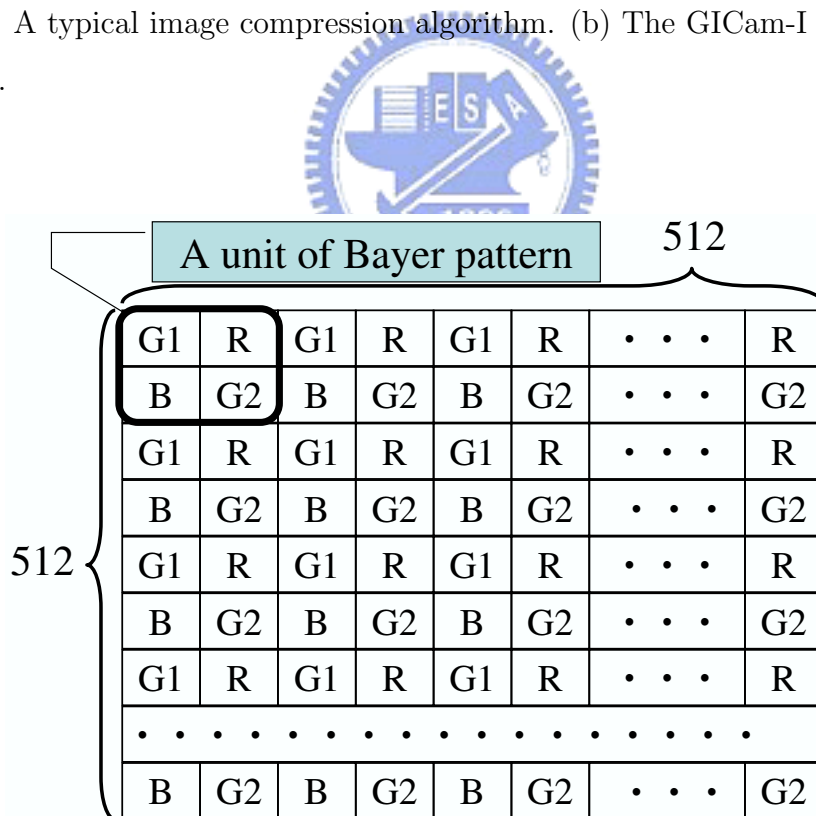
Figure 3.3. The Bayer patterns in the raw image.

R quantization table

16	16	16	16	16	32	32	64
16	16	16	16	32	32	64	64
16	16	16	16	32	32	64	128
16	16	16	16	32	64	64	128
16	32	32	32	64	64	128	128
32	32	64	64	64	128	128	128
64	64	64	128	128	128	128	256
64	64	128	128	128	256	256	256

B quantization table

32	32	32	32	64	64	128	128
32	32	32	64	64	128	128	256
32	32	32	32	64	128	256	512
32	64	64	64	128	256	256	512
64	128	64	128	256	256	512	512
128	128	128	256	256	512	512	512
128	256	256	256	512	512	512	1024
256	256	512	512	512	1024	1024	1024

G quantization table

16	16	16	16	16	32	32	32
16	16	8	16	16	16	32	32
16	8	8	16	16	32	32	64
16	8	16	32	32	32	64	64
16	16	32	32	32	64	64	64
32	16	32	32	64	64	64	64
32	32	32	64	64	64	128	128
64	64	64	128	128	128	128	128

Figure 3.4. The modified RGB quantization table.
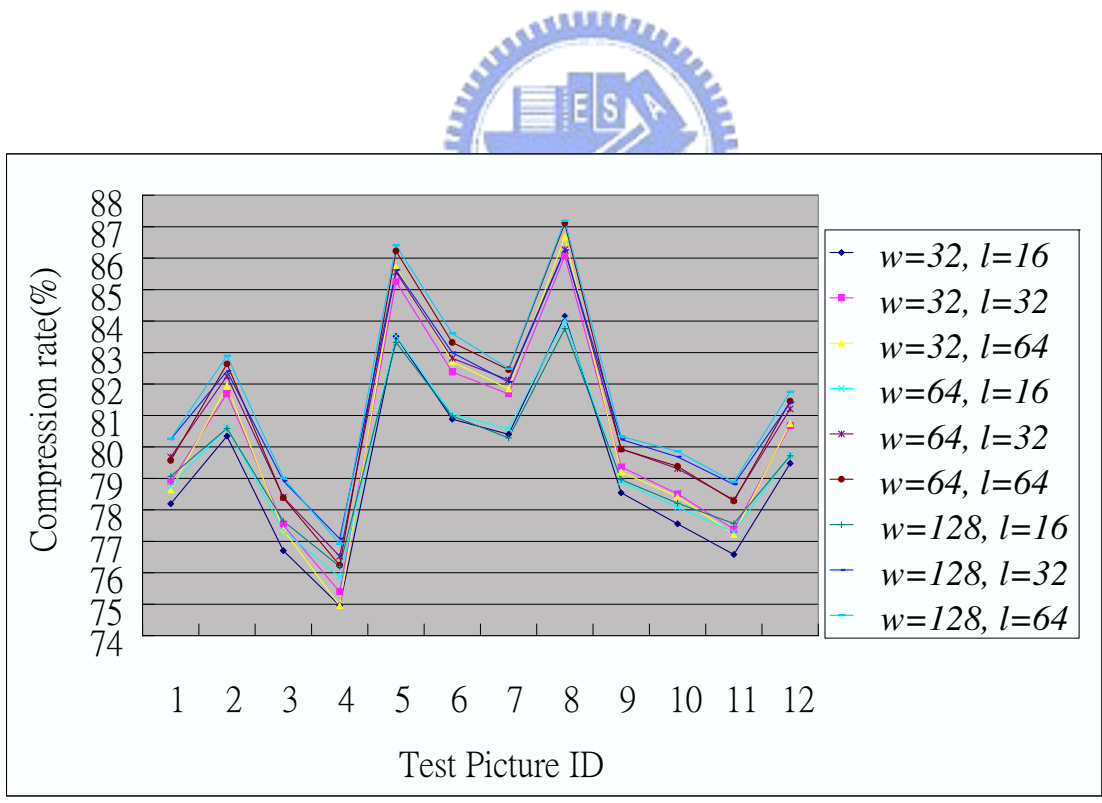
Figure 3.5. The simulation results of the GICam-I image compression.

memory compiler consume 9.40 mW. Fig.3.6 illustrates the chip layout of the GICam image compressor. The memory access dissipates the most power in GICam-I. Therefore, in order to achieve the target of expending the battery life, how to further reduce the memory access is necessary.

Technology	TSMC 0.18um 1P6M
Power Supply / Temperature	1.8V / 25° C
Chip Size	1255.24×1257.93 μm^2
Core Size	624.96×627.45 μm^2
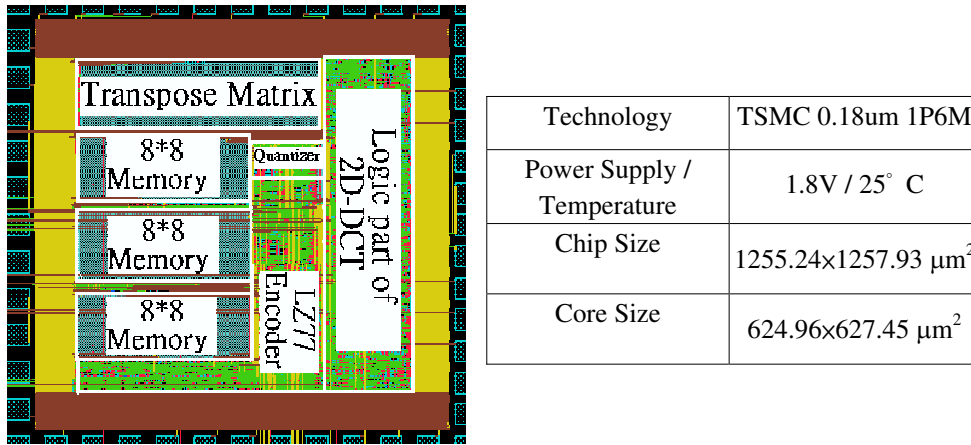
Figure 3.6. The chip layout of the GICam-I image compressor.

3.2 The Analysis of Sharpness Sensitivity In Gastrointestinal Images

From the Section 3.1, the ultra-low-power GICam-I image compressor has been successfully presented for wireless capsule endoscope. It helps the endoscope can deliver a compressed 512-by-512 image while the RF transmission rate is at 0.5 megabits per second. In applications of capsule endoscopy, it is imperative to consider battery life/performance tradeoffs. To further extend the battery life of capsule endoscope, we herein present a subsample-based GICam image compressor, called GICam-II. The proposed compression technique is motivated by the reddish feature of GI image. In order to select the desired subsample ratios to red, green and blue signals in a GI image, Subsection 3.2.1, Subsection 3.2.2 and Subsection 3.2.3 quantitatively analyze the importance of each primary colors respectively. As per the analysis of color sensitivity, the sensitivity of GI image sharpness to red component is at the same level as the sensitivity to green component. This result shows that the GI image is cardinal and different from the general image, whose sharpness sensitivity to green component is much higher than the sharpness sensitivity to red component. Because the GICam-II starts compressing the GI image from the Bayer-patterned image, the GICam-II technique subsamples the green component to make the weighting of red and green components the same. Besides, since the sharpness sensitivity to blue component is as low as 7%, the blue component is down-sampled by four. Next, Subsection 3.2.1, Subsection 3.2.2 and Subsection 3.2.3 will describe the analysis of color sensitivity in detail.

3.2.1 The Distributions of Primary Colors In The RGB Color Space

In the modern color theory [22, 23], most color spaces in used today are oriented either toward hardware design or toward product applications. Among these color spaces, the RGB(red, green, blue) space is the most commonly used in the category of digital image processing; especially, broad class of color video cameras and we consequently adopt the RGB color space to analysis the importance of primary colors in the GI images. In the

RGB color space, each color appears in its primary spectral components of red, green, and blue. The RGB color space is based on a Cartesian coordinate system and is the cube shown in Fig.3.8. In which, the differ colors of pixels are points on or inside the cube based on the triplet of values (R, G, B).

In this work, we applied twelve tested GI images shown in Fig.3.7 for testcases to evaluate the compression technique. As seen in Fig.3.9 and Fig.3.10, the distribution of GI image pixels in the RGB color space is non-uniformed. Obviously, the GI image is reddish and the pixels are amassed to the red region. Based on the observation in the RGB color space, most red values are distributed between 0.5 and 1 while most green and blue values are distributed between 0 and 0.5 for all tested GI images.
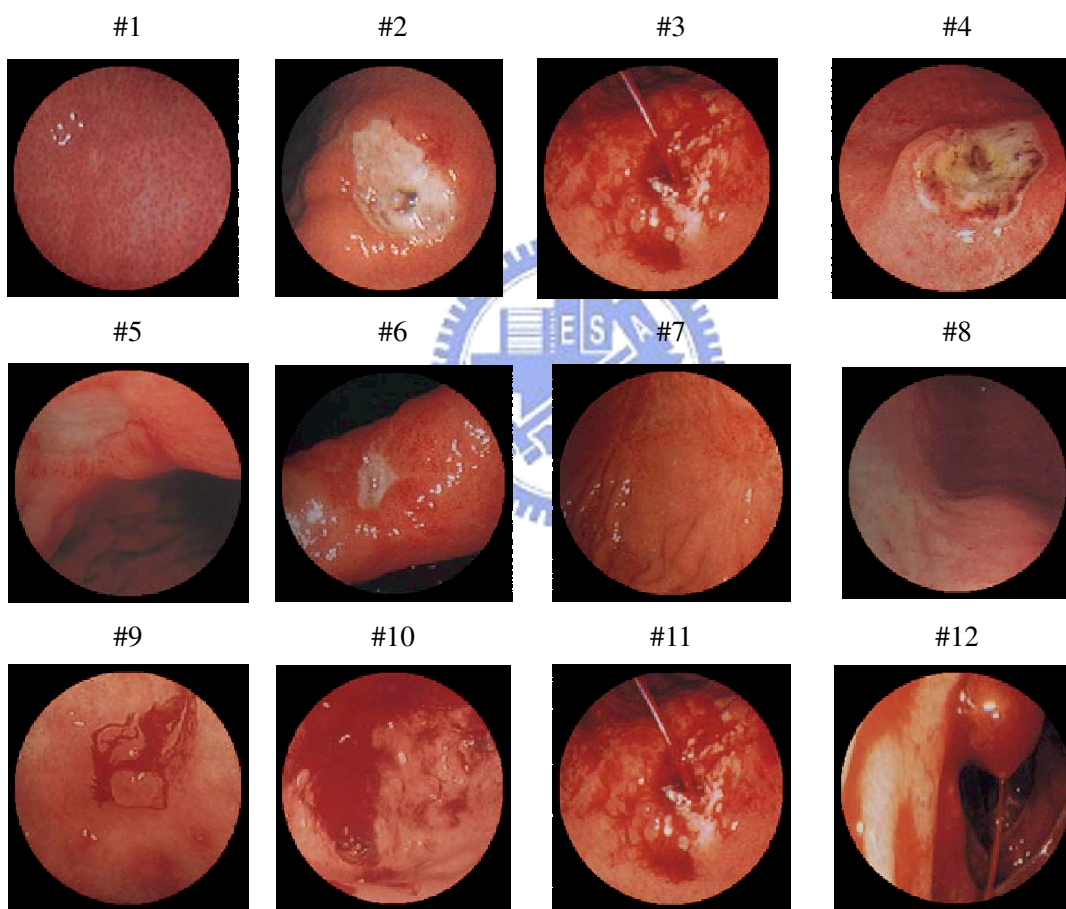
Figure 3.7. The twelve tested GI images.

To further analyze the chrominance distributions and variations in the RGB color space for each tested GI images, two quantitative indexes are used to quantify these effects. The
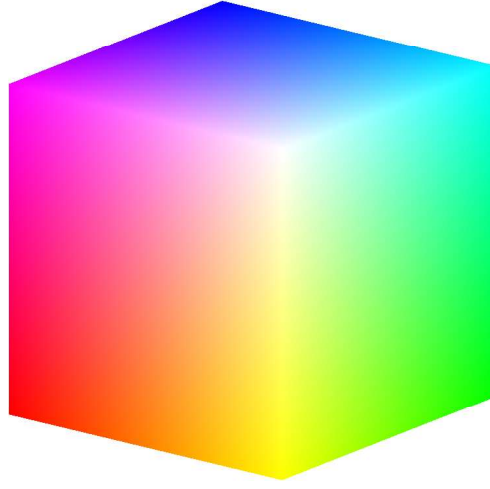
Figure 3.8. The RGB color space.

first index is to calculate the average distances between total pixels and the maximum primary colors in each GI image and the formulas are formulated as Eq.3.2.1, Eq.3.2.2 and Eq.3.2.3. First, Eq.3.2.1 defines the the average distance between total pixels and the most red color ($\overline{R}$), in which, $R(i,j)$ means the value of red component of one GI image at (i,j) position and the value of most red color (R_{max}) is 255. In addition, M and N mean the width and length for one GI image, respectively. In which, the M and the N are 512. Next, Eq.3.2.2 also defines the average distance between total pixels and the most green color ($\overline{G}$) and the value of most green one (G_{max}) is 255. Finally, Eq.3.2.3 defines the average distance between total pixels and the most blue color ($\overline{B}$) and the value of most blue color (B_{max}) is 255. Table 3.1 shows the statistical results of $\overline{R}$, $\overline{G}$ and $\overline{B}$ for all tested GI images. From Table 3.1, the results clearly show that $\overline{R}$ is the shortest average distance than $\overline{G}$ and $\overline{B}$. Therefore, human eyes can be very sensitive to the obviously cardinal ingredient on all surfaces of tested GI images. Moreover, comparing $\overline{G}$ with $\overline{B}$, $\overline{G}$ is shorter than $\overline{B}$ because $\overline{G}$ contributes larger proportion in luminance.

$$
\begin{aligned}
\overline{R} &= E[(1 - \tfrac{R(i,j)}{R_{max}})] \\
&= (\tfrac{1}{M \times N}) \sum_{i=0}^{M-1} \sum_{j=0}^{N-1} (1 - \tfrac{R(i,j)}{R_{max}})
\end{aligned}
\tag{3.2.1}
$$

$$
\begin{aligned}
\overline{G} &= E[(1 - \tfrac{G(i,j)}{G_{max}})] \\
&= (\tfrac{1}{M \times N}) \sum_{i=0}^{M-1} \sum_{j=0}^{N-1} (1 - \tfrac{G(i,j)}{G_{max}})
\end{aligned}
\tag{3.2.2}
$$

19
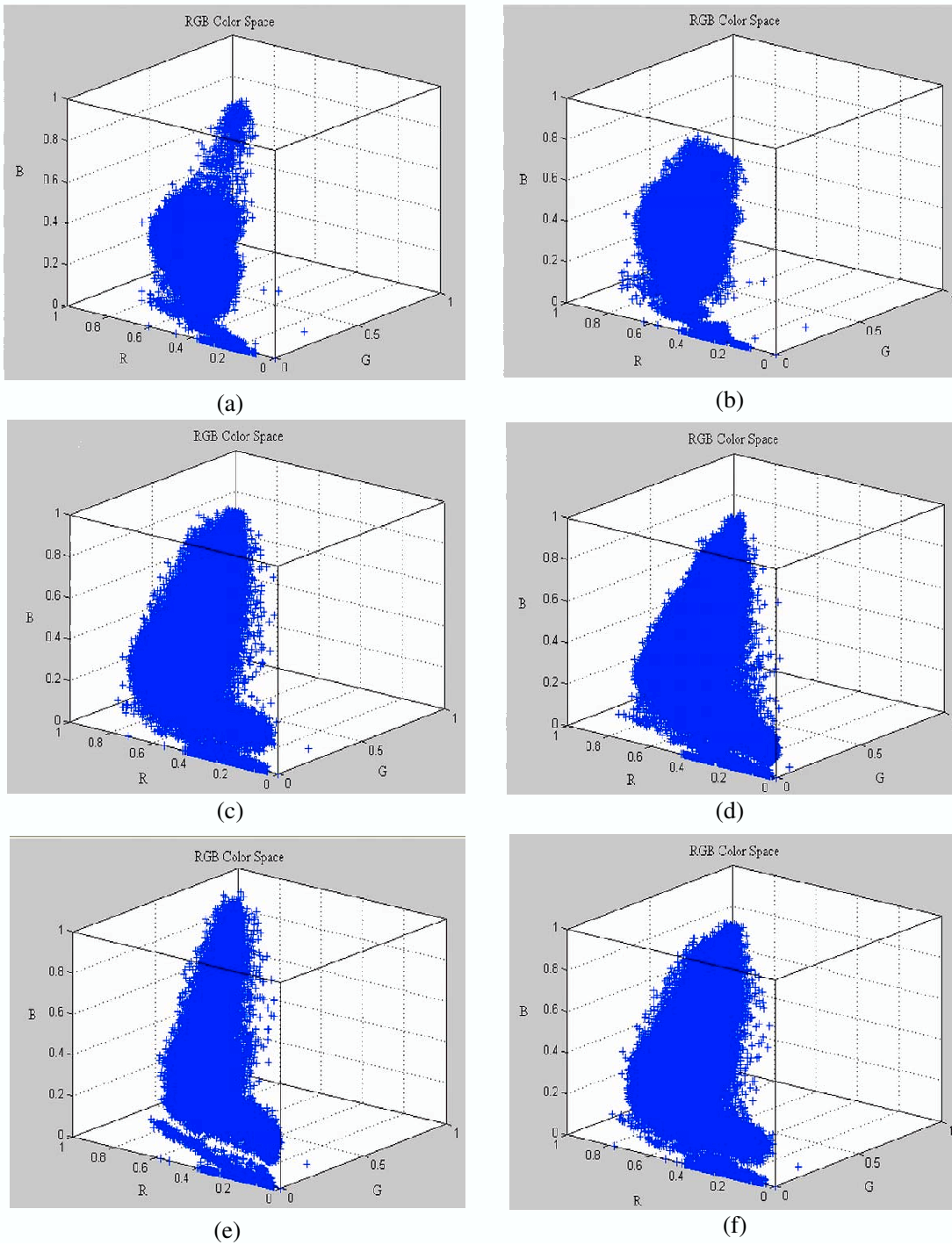
Figure 3.9. (a) The RGB color space distribution for 1st tested GI image. (b) The RGB color space distribution for 2nd tested GI image. (c)The RGB color space distribution for 3rd tested GI image. (d) The RGB color space distribution for 4th tested GI image. (e) The RGB color space distribution for 5th tested GI image. (f) The RGB color space distribution for 6th tested GI image.
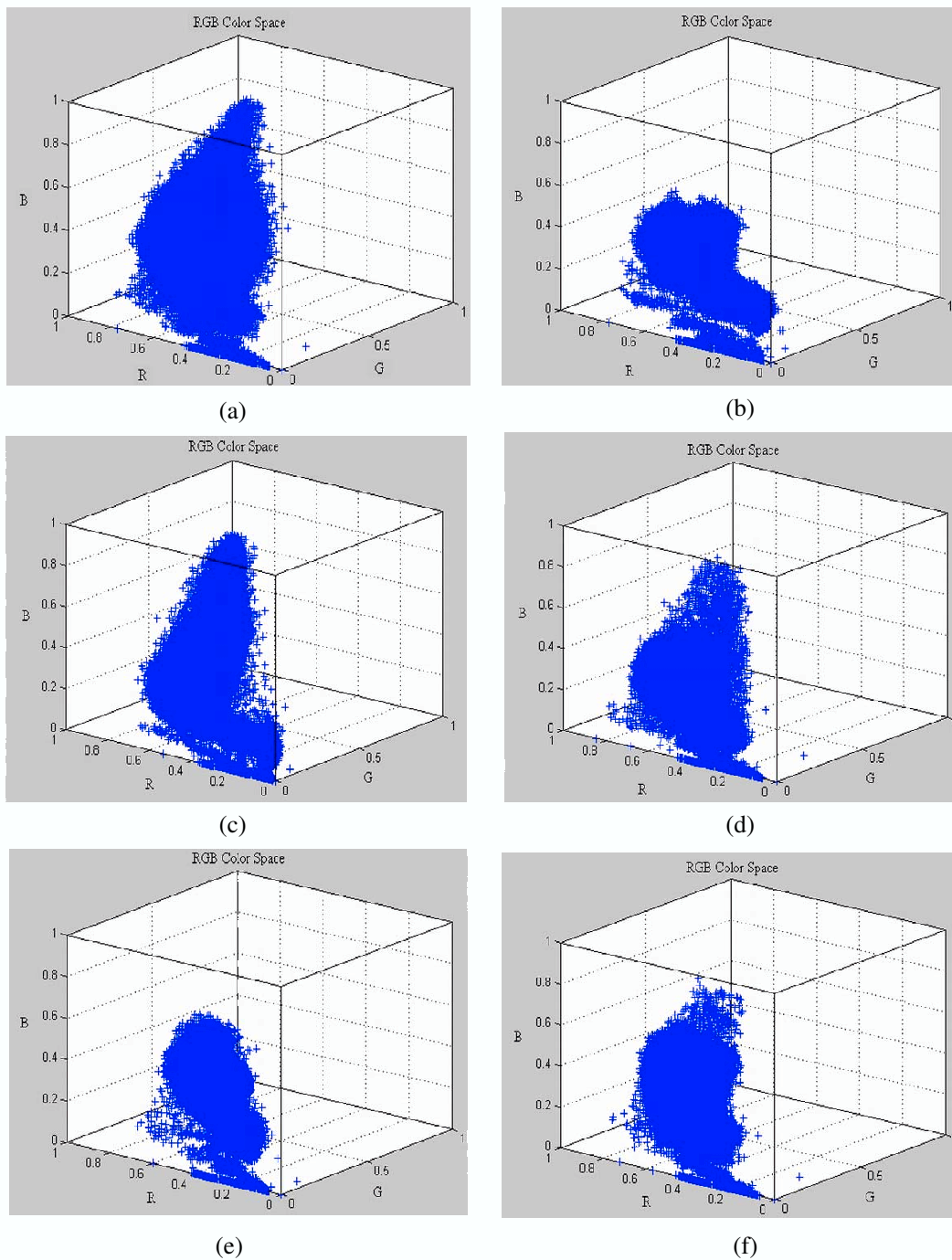
Figure 3.10. (a) The RGB color space distribution for 7th tested GI image. (b) The RGB color space distribution for 8th tested GI image. (c)The RGB color space distribution for 9th tested GI image. (d) The RGB color space distribution for 10th tested GI image. (e) The RGB color space distribution for 11th tested GI image. (f) The RGB color space distribution for 12th tested GI image.

$$\overline{B} = E[(1 - \frac{B(i,j)}{B_{max}})]$$
$$= (\frac{1}{M \times N}) \sum_{i=0}^{M-1} \sum_{j=0}^{N-1} (1 - \frac{B(i,j)}{B_{max}}) \qquad (3.2.3)$$

Table 3.1. The analysis of average distance.

Average Distance			
Test Picture ID	$\overline{R}$	$\overline{G}$	$\overline{B}$
1	0.58	0.80	0.82
2	0.55	0.74	0.79
3	0.54	0.81	0.86
4	0.55	0.76	0.81
5	0.66	0.82	0.85
6	0.66	0.84	0.87
7	0.59	0.82	0.88
8	0.68	0.81	0.83
9	0.55	0.80	0.85
10	0.53	0.81	0.84
11	0.53	0.81	0.86
12	0.62	0.80	0.85
Average	0.59	0.80	0.84

The first index has been particularly quantified the chrominance distributions through the concept of average distance and the statistical results have also been shown that the reason why the human eye can sense the obviously cardinal ingredient for all tested GI images. Next, the second index is to calculate the variance between total pixels and average distance in order to further observe the color variations in GI images and the formulas are formulated as Eq.3.2.4, Eq.3.2.5 and Eq.3.2.6. The Table 3.2 shows that the average variation of red signal is 0.09, the average variance of green one is 0.03, and the average variance of blue one is 0.02. It signifies that the color information of red signal needs to be preserved carefully more than another two primary colors; green and blue for GI images because the dynamic range of red signal is broader than green and blue ones. In addition,

The secondary is green signal and the last is blue signal.

$$VAR_R = E[(1 - \frac{R(i,j)}{R_{max}})^2] - \{E[(1 - \frac{R(i,j)}{R_{max}})]\}^2$$
$$= (\frac{1}{M \times N}) \sum_{i=0}^{M-1} \sum_{j=0}^{N-1} [1 - \frac{R(i,j)}{R_{max}}]^2 -$$
$$[(\frac{1}{M \times N}) \sum_{i=0}^{M-1} \sum_{j=0}^{N-1} (1 - \frac{R(i,j)}{R_{max}})]^2$$

(3.2.4)

$$VAR_G = E[(1 - \frac{G(i,j)}{G_{max}})^2] - \{E[(1 - \frac{G(i,j)}{G_{max}})]\}^2$$
$$= (\frac{1}{M \times N}) \sum_{i=0}^{M-1} \sum_{j=0}^{N-1} [1 - \frac{G(i,j)}{G_{max}}]^2 -$$
$$[(\frac{1}{M \times N}) \sum_{i=0}^{M-1} \sum_{j=0}^{N-1} (1 - \frac{G(i,j)}{G_{max}})]^2$$

(3.2.5)

$$VAR_B = E[(1 - \frac{B(i,j)}{B_{max}})^2] - \{E[(1 - \frac{B(i,j)}{B_{max}})]\}^2$$
$$= (\frac{1}{M \times N}) \sum_{i=0}^{M-1} \sum_{j=0}^{N-1} [1 - \frac{B(i,j)}{B_{max}}]^2 -$$
$$[(\frac{1}{M \times N}) \sum_{i=0}^{M-1} \sum_{j=0}^{N-1} (1 - \frac{B(i,j)}{B_{max}})]^2$$

(3.2.6)

3.2.2 The Analysis of Sharpness Sensitivity to Primary Colors for Gastrointestinal Images

Based on the analysis of RGB color space, the importance of chrominance is quantitatively demonstrated for GI images. Expect the chrominance, the luminance is another important index because it can efficiently represent a sharpness of object. Eq.3.2.7 is the formula of luminance (Y) and the parameters ; a1, a2 and a3 are 0.299, 0.587 and 0.114 respectively.

$$Y = a1 \times R + a2 \times G + a3 \times B$$

(3.2.7)

To efficiently analyze the importance of primary colors in the luminance, the analysis of sensitivity is applied. Through the analysis of sensitivity, the variation of luminance can actually reflect the influence of each primary colors. Eq.3.2.8, Eq.3.2.9 and Eq.3.2.10 define

Table 3.2. The analysis of variance.

Variance of Distance			
Test Picture ID	VAR_R	VAR_G	VAR_B
1	0.08	0.02	0.02
2	0.11	0.05	0.03
3	0.10	0.03	0.02
4	0.10	0.04	0.02
5	0.07	0.02	0.01
6	0.08	0.02	0.01
7	0.09	0.02	0.01
8	0.06	0.02	0.02
9	0.09	0.03	0.01
10	0.10	0.03	0.02
11	0.10	0.03	0.02
12	0.10	0.04	0.02
Average	0.09	0.03	0.02

the sensitivity of red $(S_{Y_{i,j}}^{R_{i,j}})$, the sensitivity of green $(S_{Y_{i,j}}^{G_{i,j}})$ and the sensitivity of blue $(S_{Y_{i,j}}^{B_{i,j}})$ at position (i,j) respectively for a color pixel of a GI image.

$$S_{Y_{i,j}}^{R_{i,j}} = \frac{\Delta Y_{i,j}/Y_{i,j}}{\Delta R_{i,j}/R_{i,j}} = \frac{R_{i,j}}{Y_{i,j}} \times \frac{\Delta Y_{i,j}}{\Delta R_{i,j}} = \frac{a1 \times R_{i,j}}{Y_{i,j}}$$

(3.2.8)

$$S_{Y_{i,j}}^{G_{i,j}} = \frac{\Delta Y_{i,j}/Y_{i,j}}{\Delta G_{i,j}/G_{i,j}} = \frac{G_{i,j}}{Y_{i,j}} \times \frac{\Delta Y_i}{\Delta G_{i,j}} = \frac{a2 \times G_{i,j}}{Y_{i,j}}$$

(3.2.9)

$$S_{Y_{i,j}}^{B_{i,j}} = \frac{\Delta Y_{i,j}/Y_{i,j}}{\Delta B_{i,j}/B_{i,j}} = \frac{B_{i,j}}{Y_{i,j}} \times \frac{\Delta Y_i}{\Delta B_{i,j}} = \frac{a3 \times B_{i,j}}{Y_{i,j}}$$

(3.2.10)

After calculating the sensitivity of each primary colors for a GI image, the average sensitivity of red $(\overline{S_Y^R})$, the average sensitivity of green $(\overline{S_Y^G})$ and the average sensitivity of blue $(\overline{S_Y^B})$ are calculated by Eq.3.2.11, Eq.3.2.12 and Eq.3.2.13 for each GI images. Where, M and N means the width and length for a GI image, respectively. Table 3.3 shows the

average sensitivities of red, green and blue for all tested GI images. From the calculational results, the sensitivity of blue is slightest and hence the variation of luminance arising from the aliasing of blue is very invisible. In addition to the sensitivity of blue, the sensitivity of red is close to the one of green and thus they both have the very close influence on the variation of luminance.

$$\overline{S_Y^R} = \left(\frac{1}{M \times N}\right) \sum_{i=0}^{M-1} \sum_{j=0}^{N-1} S_{Y_{i,j}}^{R_{i,j}} \tag{3.2.11}$$

$$\overline{S_Y^G} = \left(\frac{1}{M \times N}\right) \sum_{i=0}^{M-1} \sum_{j=0}^{N-1} S_{Y_{i,j}}^{G_{i,j}} \tag{3.2.12}$$

$$\overline{S_Y^B} = \left(\frac{1}{M \times N}\right) \sum_{i=0}^{M-1} \sum_{j=0}^{N-1} S_{Y_{i,j}}^{B_{i,j}} \tag{3.2.13}$$

To sum up the variance of chrominance and the sensitivity of luminance, the blue is

Table 3.3. Sensitivities of red, green and blue for all tested GI images.

The sensitivity of primary colors in luminance			
Test Picture ID	$\overline{S_Y^R}$	$\overline{S_Y^G}$	$\overline{S_Y^B}$
1	0.49	0.43	0.08
2	0.44	0.48	0.08
3	0.55	0.39	0.06
4	0.47	0.46	0.07
5	0.45	0.47	0.08
6	0.48	0.45	0.07
7	0.52	0.42	0.06
8	0.44	0.48	0.08
9	0.51	0.43	0.06
10	0.54	0.40	0.06
11	0.55	0.39	0.06
12	0.49	0.44	0.07
Average	0.49	0.44	0.07

the most insensitive color in the GI images. Therefore, the blue component can be further downsampled without significant sharpness degradation. Moreover, comparing the red

signal with the green signal, they both have the very close influence on the variation of luminance because of both having very close sensitivities. However, the chrominance of red varies more violent than the chrominance of green and hence the information completeness of red has higher priority than the green. Due to the proposed compression coding belongs to the DCT-based image coding, the coding is processed in the spatial-frequency domain. To let the priority relationship between red and green also response in the spatial-frequency domain, the analysis of alternating current (AC) variance will be accomplished to demonstrate the inference mentioned above in the next subsection.

3.2.3 The Analysis of AC Variance In The 2-D DCT Spatial Frequency Domain For Gastrointestinal Images

According to the analysis results from the distributions of primary colors in the RGB color space and the proportion of primary colors in the luminance for GI images, the red signal plays a decisive role in the raw image. The green signal plays a secondary role and the blue signal is very indecisive. To verify the validity of observation mentioned above, we first use the two-dimensional (2-D) 8×8 discrete cosine transform (DCT) to transfer the spatial domain into the spatial-frequency domain for each of R, G1, G2 and B components. The 2-D 8×8 DCT transformation can be view as the process of finding for each waveform in the 2-D 8×8 DCT basic functions and also can be formulated as Eq.3.2.14, Eq.3.2.15, Eq.3.2.16, Eq.3.2.17 and Eq.3.2.18 for each 8×8 block in R, G1, G2 and B subimages respectively. Where, M and N mean the width and length for one GI image respectively. k, l=0, 1, ..., 7 and y_{kl} is the corresponding weight of DCT basic function in the kth row and the lth column. P means the total number of pictures and B means the total number of 8×8 blocks in a GI images.

$$R_{pb}(kl) = \frac{c(k)}{2} \sum_{i=0}^{7} [\frac{c(l)}{2} \sum_{j=0}^{7} r_{ij} cos(\frac{(2j+1)l\pi}{16})] cos(\frac{(2i+1)k\pi}{16}) \qquad (3.2.14)$$

$$G_{pb}(kl) = \frac{c(k)}{2} \sum_{i=0}^{7} [\frac{c(l)}{2} \sum_{j=0}^{7} g_{ij} cos(\frac{(2j+1)l\pi}{16})] cos(\frac{(2i+1)k\pi}{16}) \qquad (3.2.15)$$

$$B_{pb}(kl) = \frac{c(k)}{2} \sum_{i=0}^{7} [\frac{c(l)}{2} \sum_{j=0}^{7} b_{ij} cos(\frac{(2j+1)l\pi}{16})] cos(\frac{(2i+1)k\pi}{16}) \qquad (3.2.16)$$

26

$$c(k) = \begin{cases} \frac{1}{\sqrt{2}}, & if\ k = 0 \\ 1, & otherwise. \end{cases} \qquad (3.2.17)$$

$$c(l) = \begin{cases} \frac{1}{\sqrt{2}}, & if\ l = 0 \\ 1, & otherwise. \end{cases} \qquad (3.2.18)$$

Next, we also calculate the average energy amplitude of all alternating current (AC) coefficients of all tested GI images in order to particularity observe the variation of energy for each of R, G1, G2 and B components and the calculations are formulated as Eq.3.2.19, Eq.3.2.20, Eq.3.2.21.

$$A_R(kl) = \frac{1}{P} \sum_{p=1}^{P} \left[\sum_{b=0}^{B-1} |R_{pb}(kl)| \right] \qquad (3.2.19)$$

$$A_G(kl) = \frac{1}{P} \sum_{p=1}^{P} \left[\sum_{b=0}^{B-1} |G_{pb}(kl)| \right] \qquad (3.2.20)$$

$$A_B(kl) = \frac{1}{P} \sum_{p=1}^{P} \left[\sum_{b=0}^{B-1} |B_{pb}(kl)| \right] \qquad (3.2.21)$$

After calculating the average energy amplitude, we convert the 2-D DCT domain into the one-dimensional (1-D) signal distribution in order to conveniently observe the variation of frequency. Consequently, a tool to transform two-dimensional signals into one dimension is needed. There are many schemes to convert 2-D into 1-D, including row-major scan, column-major scan, peano-scan, and zig-zag scan. Almost all the DCT coding schemes adopt zigzag scan to accomplish the goal of conversion, and we use it here. The benefit of zig-zag is its property of compacting energy to low frequency regions after discrete cosine transformation. The arrangement sorts the coefficients from low to high frequency and Fig.3.11(a) the shows the zig-zag scanning order for 8×8 block. Fig.3.11(b) shows the 1-D signal distribution after Zigzag scanning order and Fig.3.11(c) shows the symmetric type of frequency for the 1-D signal distribution.

Through the converting method of Fig.3.11, the 1-D signal distributions of each R, G1, G2, B components are shown in Fig.3.12. The variances of frequency are 1193, 1192, 1209 and 1244 for G1, G2, R and B respectively and the variance of R are very close to the ones

27

(a)

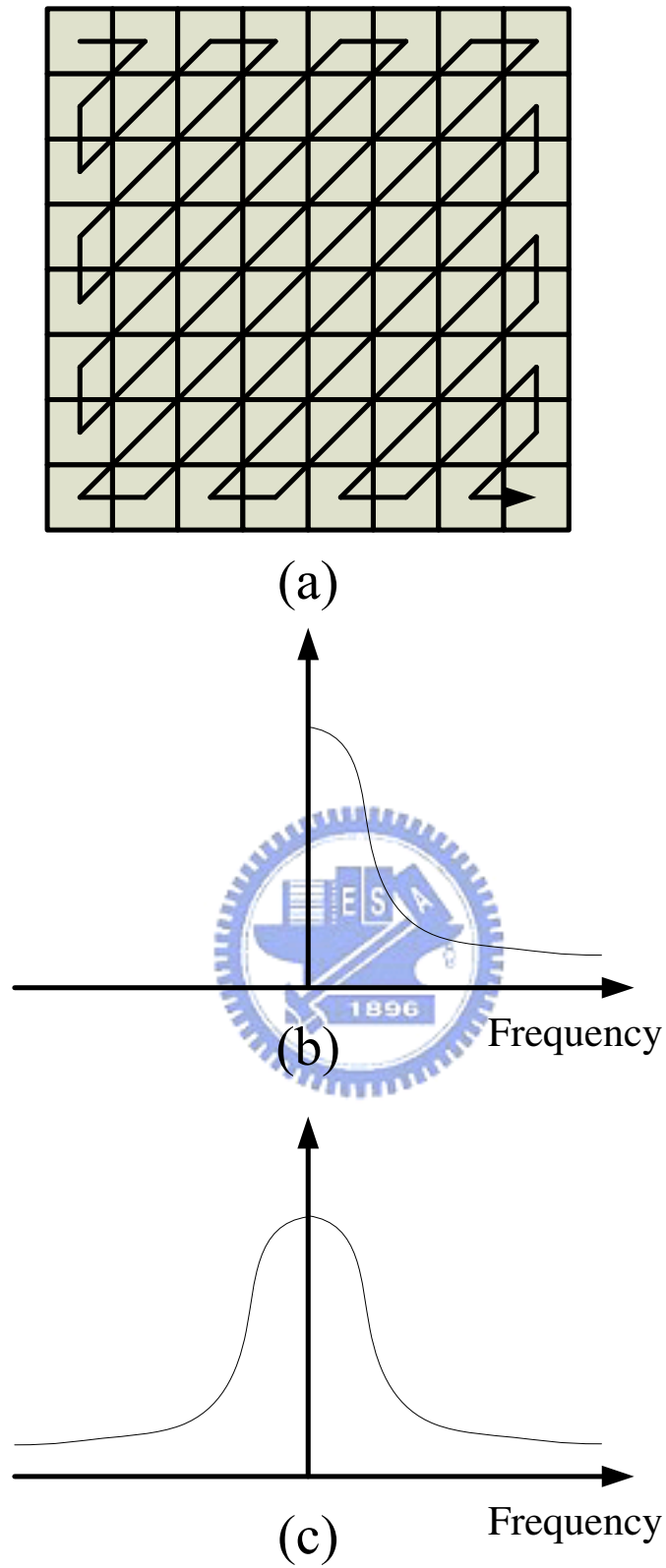(b)   Frequency

(c)   Frequency

Figure 3.11. (a) zig-zag scanning for 8×8 block. (b) 1-D signal distribution after zig-zag scanning order. (c) The symmetric type of frequency for the 1-D signal distribution.
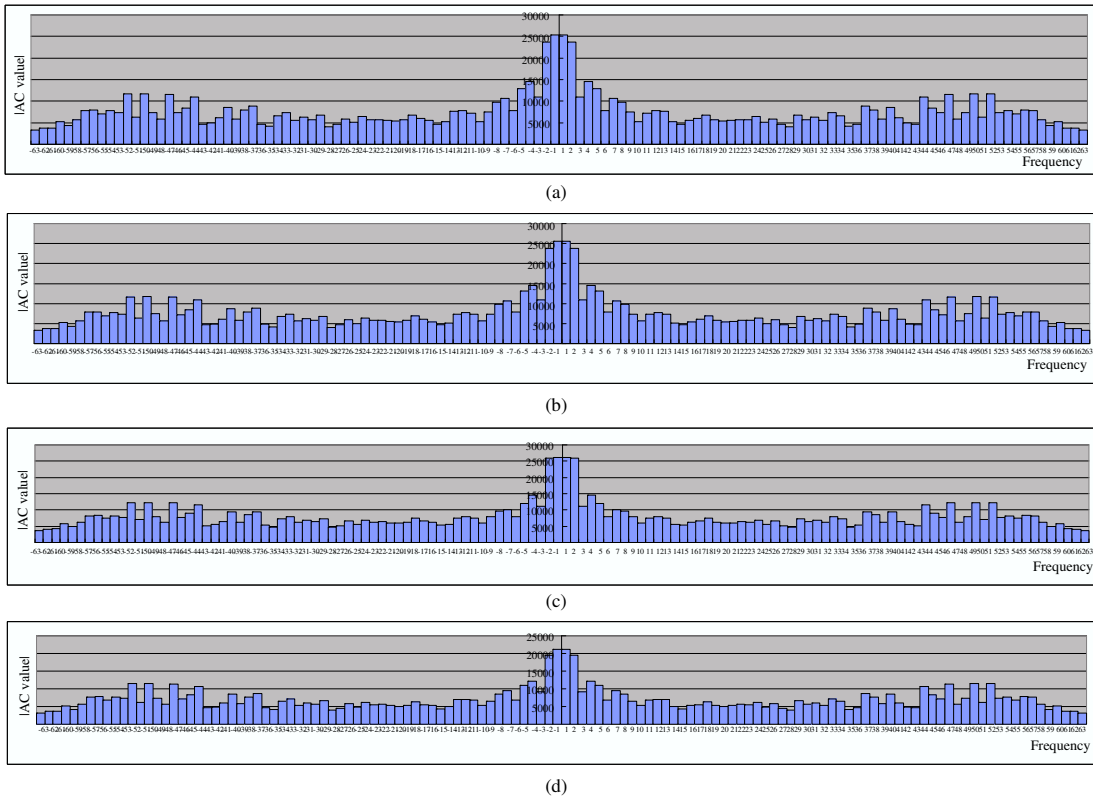
Figure 3.12. (a) Spatial-frequency distribution converting into one-dimension for g1. (b) Spatial-frequency distribution converting into one-dimension for g2. (c) Spatial-frequency distribution converting into one-dimension for r. (d) Spatial-frequency distribution converting into one-dimension for b.

of G1 and G2 from the result. However, the datum of G are twice the datum of R based on the Bayer pattern and hence the datum of G can reduce half at most.

Based on the analysis result mentioned above, the R component is very decisive for GI images and it needs to be compressed completely. However, the G1, G2 and B components do not need to be compressed completely because their importance are less than the R component. Therefore, in order to efficiently reduce the memory access to expend the battery life of capsule endoscopy, the datum of G1, G2 and B components should be appropriately decreased according to the proportion of their importance before the compression process. We successfully propose a subsample-based GICam image compression algorithm, called GICam-II and this proposed algorithm firstly uses the subsample technique to reduce the incoming datum of G1, G2 and B components before compression process. Section 3.3 will describe the proposed algorithm in detail.

29

3.3 The Subsample-Based GICam Image Compression Algorithm (GICam-II)

Fig.3.13 illustrates the GICam-II compression algorithm. For a 512×512 raw image, the raw image firstly divides into four parts, namely, R, G1, G2, B components and each of R, G1, G2, and B components has 256×256 pixels. For the R component, the incoming image size to the 2D-DCT is 256×256×8 bits, in which, the incoming image datum are completely compressed because of the importance itself in GI images. Except the R component, the
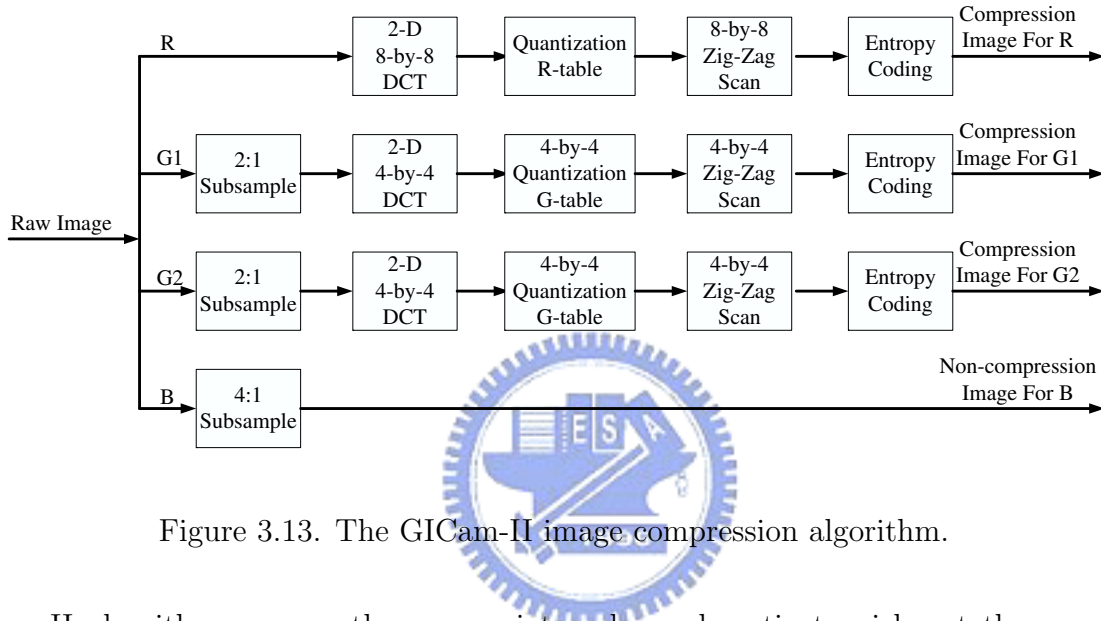

Figure 3.13. The GICam-II image compression algorithm.

GICam-II algorithm can use the appropriate subsample ratio to pick out the necessary image pixels into the compression process for G1, G2 and B components and Eq.3.3.22 and Eq.3.3.23 are formulas for the subsample technique. Where, $SM_{16:2m}$ is the subsample mask for the subsample ratio 16-to-2m as shown in Eq.3.3.22 and the subsample mask $SM_{16:2m}$ is generated from basic mask as shown in Eq.3.3.23. The type of subample direction is block-based, when certain of positions in the subsample mask are one, their pixels in the same position will be compressed, otherwise they are not processed. For the G1 and G2 components, the low subsample ratio needs to be assigned because of considering their secondary importance in GI images. Thus, the 2:1 subsample ratio is the candidate one and the subsample pattern is shown in Fig.3.14 (a). Finally, for the B component, the 4:1 subsample ratio is assigned and the subsample pattern is shown in Fig.3.14 (b). In the GICam-II image compression algorithm, the 8×8 2D-DCT is still used to transfer the R

component. However, the 4×4 2D-DCT is used for G1 and G2 components because the incoming datum are reduced by subsample technique. Moreover, the G quantization table is also further modified and shown in the Fig.3.15. Finally, the B component is directly transmitted; not be compressed, after extremely decreasing the incoming datum. Due to non-compression for the B component, the 8×8 and 4×4 Zig-Zag scanning techniques are added into the GICam-II to further increase the compression rate for R, G1 and G2 components before entering the entropy encoding. In the GICam-II, the Lempel-Ziv (LZ) coding [24] is also employed for the entropy coding because of non-look-up tables and low complex computation.

$$SM_{16:2m}\left(i,j\right) = BM_{16:2m}\left(i \mod 4, j \mod 4\right)$$

$$m = 1, 2, 3, 4, 5, 6, 7, 8. \tag{3.3.22}$$

$$BM_{16:2m} =$$
$$\begin{bmatrix} u\left(m-1\right) & u\left(m-5\right) & u\left(m-2\right) & u\left(m-6\right) \\ u\left(m-7\right) & u\left(m-3\right) & u\left(m-8\right) & u\left(m-4\right) \\ u\left(m-2\right) & u\left(m-5\right) & u\left(m-1\right) & u\left(m-6\right) \\ u\left(m-7\right) & u\left(m-3\right) & u\left(m-8\right) & u\left(m-4\right) \end{bmatrix} \tag{3.3.23}$$

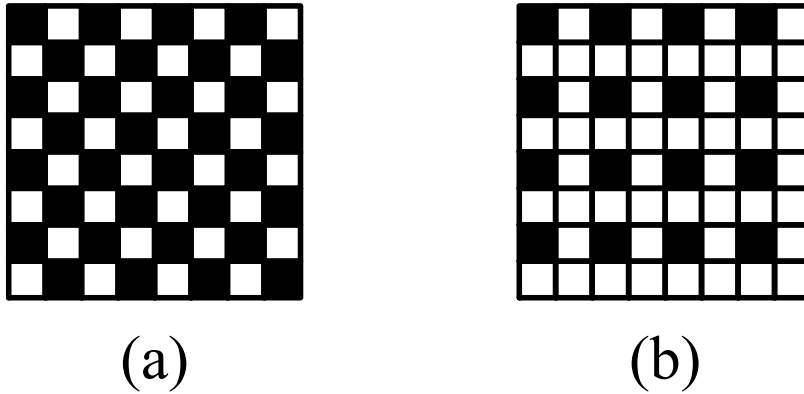where $u(n)$ is a step function, $u\left(n\right) = \begin{cases} 1, & for\ n \geq 0 \\ 0, & for\ n < 0. \end{cases}$

(a)   (b)

Figure 3.14. (a) 2:1 subsample pattern. (b) 4:1 subsample pattern.

16	16	16	16	16	32	32	64
16	16	16	16	32	32	64	64
16	16	16	16	32	32	64	128
16	16	16	16	32	64	64	128
16	32	32	32	64	64	128	128
32	32	64	64	64	128	128	128
64	64	64	128	128	128	128	128
64	64	128	128	128	128	128	128

16	8	32	32
16	16	32	64
32	32	64	64
64	64	128	128

(a) (b)

Figure 3.15. (a)The modified R quantization table. (b) The modified G quantization table.

3.4   Experimental Results

In Section 3.3, we have particularly introduced how to efficiently decrease the incoming datum with the subsmaple technique in the GICam-II compression algorithm and then the GICam-II compressor will be experimentally analyzed the performance about the compression rate, the quality degradation and the ability of power saving.

3.4.1   The Analysis of Compression Rate for Gastrointestinal Images

There are twelve GI images are tested and shown in the Fig.3.7. First of all, the target compression performance of the GICam-II image compression is to reduce image size by 75% at least. To meet the specification, we have to exploit the cost-optimal LZ coding parameters. There are two parameters in the LZ coding to be determined; they are the window size, w, and the maximum matching length,l. The larger the parameters, the higher the compression ratio but the higher the implementation cost. In addition, there are two kinds of LZ codings in the GICam-II compressor, one is R(w, l) for R component and the other is G(w, l) for G1 and G2 components. We set the values of parameters by using the compression ratio of 4:1 as the threshold. Our goal is to determine the minimum R(w, l)

and G(w, l) sets under the constraint of 4:1 compression ratio.

The compression ratio (CR) is defined as the ratio of the raw image size to the compressed image size and formulated as Eq.3.4.24. The measure of the compression ratio is the compression rate. The formula of the compression rate is calculated by Eq.3.4.25. The results in Fig.3.16 are shown by simulating the behavior model of GICam-II compressor; it is generated by MATLAB. As seen in Fig.3.16, simulating with 12 endoscopic pictures, (32, 32) and (16, 8) are the minimum R(w, l) and G(w, l) sets to meet the compression ratio requirement.

$$Compression\ Ratio\ (CR) = \frac{bits\ before\ compression}{bits\ after\ compression} \tag{3.4.24}$$

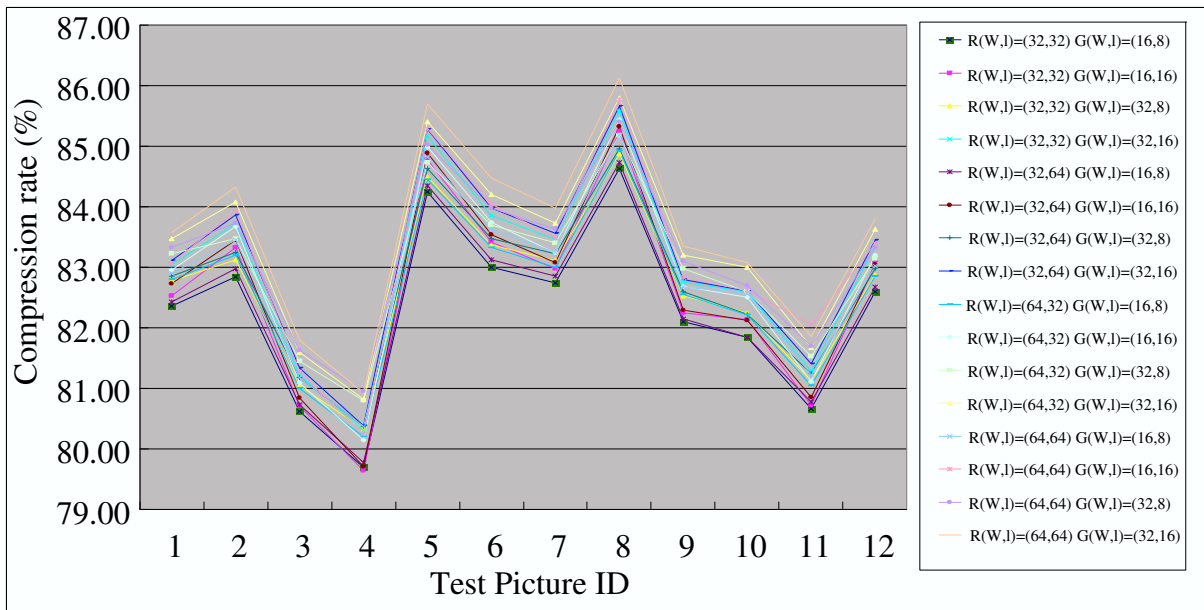$$Compression\ Rate = (1 - CR^{-1}) \times 100\% \tag{3.4.25}$$

Figure 3.16. The simulation results of the GICam-II image compression.

3.4.2 The Analysis of Compression Quality for Gastrointestinal Images

Using (32, 32) and (16, 8) as the parameter sets, in Table 3.4, we can see the performance in terms of the quality degradation and compression ratio. The measure of compression quality is the peak signal-to-noise ratio of luminance (PSNRY). The calculation of PSNRY is formulated as Eq.3.4.26. Where MSE is the mean square error of decompressed image and is formulated as Eq.3.4.27. In Eq.3.4.27, α_{ij} is the luminance value of original GI image and β_{ij} is the luminance value of decompressed GI image. The result shows that the degradation of decompressed images is quite low while the average PSNRY is 40.73 dB. According to the objective criterion of gastroenterology doctors, the PSNRY higher than 38 dB is acceptable. To demonstrate the results, Fig.3.17 illustrates the compression quality of decoded test pictures. The difference between the original image and the decompressed image is invisible.

In addition, five professional gastroenterology doctors in the Division of Gastroenterology, Taipei Medical University Hospital are invited to verify whether the qualities of these decoded image quality are suitable for practical diagnosis and they are Dr. Shiann Pan, Dr. Jean-Dean Liu, Dr. Chun-Chao Chang, Dr. Jen-Juh Wang and Dr. Lou-Horng Yuan individually. The method of evaluation is shown in Table 3.5. The score between 0 and 2 means that the diagnosis is affected, The score between 3 and 5 means that the diagnosis is slightly affected and the score between 6 and 9 means that the diagnosis is not affected. According to the evaluation results of Fig.3.18, all decoded GI images are very suitable for practical diagnosis because of high evaluation score and the diagnoses are absolutely not affected except the 5th and 8th decoded images. The degree of diagnoses are between no affection and extremely slight affection for the 5th and the 8th decoded images. This is because two doctors subjectively feel their diagnoses are slightly affected. However, these two decoded images are not mistook in diagnosis completely for these professional gastroenterology doctors.

$$PSNRY = 10log_{10}(\tfrac{255^2}{MSE}) \tag{3.4.26}$$

$$MSE = \left(\frac{1}{M \times N}\right) \sum_{i=0}^{M-1} \sum_{j=0}^{N-1} (\alpha_{ij} - \beta_{ij})^2 \qquad (3.4.27)$$

Table 3.4. The simulation results of twelve tested GI images.

Test Picture ID	PSNRY (dB)	Compression rate (%)
1	40.76	82.36
2	41.38	82.84
3	39.39	80.62
4	38.16	79.70
5	42.56	84.25
6	41.60	83.00
7	41.03	82.74
8	43.05	84.63
9	40.21	82.11
10	40.36	81.84
11	39.39	80.66
12	40.85	82.60
Average	40.73	82.28

Table 3.5. The score of evaluation.

Score	Description
$0 \sim 2$	diagnosis is affected
$3 \sim 5$	diagnosis is slightly affected
$6 \sim 9$	diagnosis is not affected

3.4.3 The Implementation and The Analysis of Power Saving

Fig.3.19 shows the architecture of the GICam-II image compressor. The GICam-II image compressor processes the image in the order of G1, R, G2 and B. Because the data
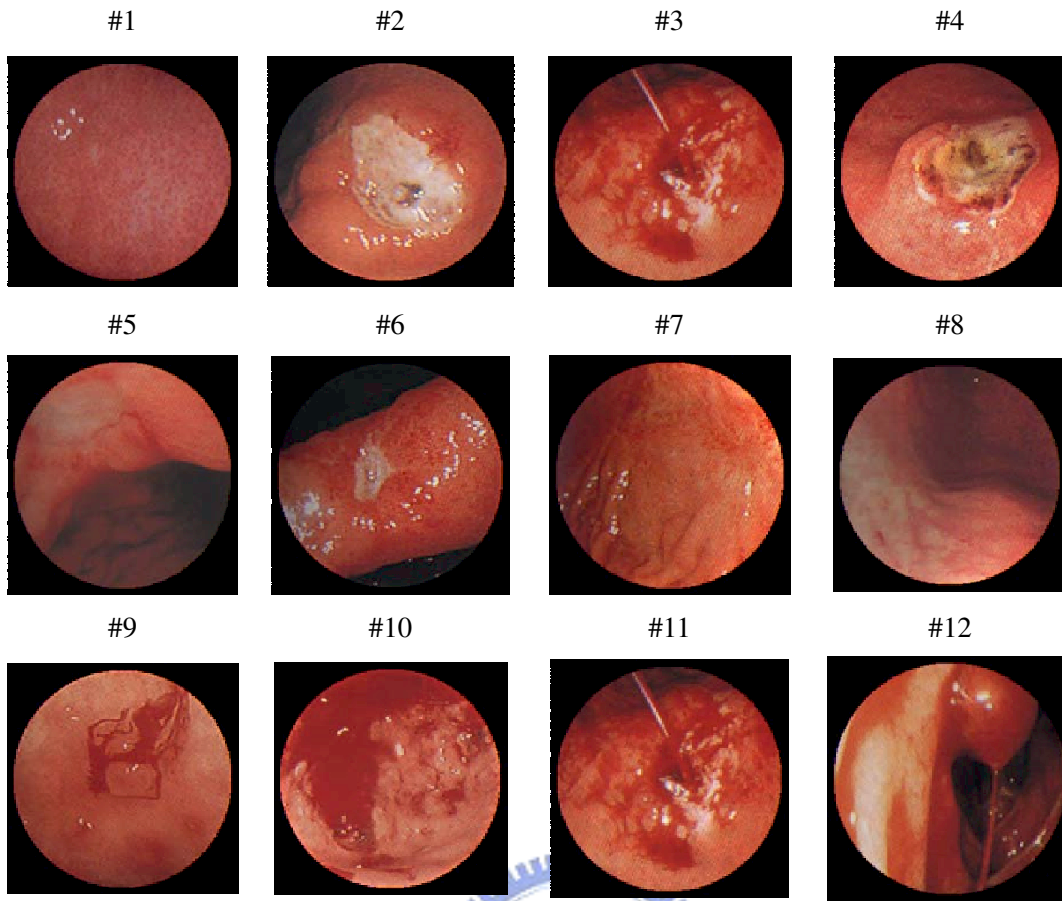
Figure 3.17. Demosaicked GI images.

stream from the image sensor is block-based, the GICam-II image compressor requires intermediate memory units to hold each block of data. To validate the GICam-II image processor, we used the FPGA board of Altera APEX 2100 K to verify the function of the GICam-II image processor and the prototype is shown in Fig.3.20. After FPGA verification, we used the TSMC 0.18 μm 1P6M process to implement the GICam-II image compressor. When operating at 1.8 V, the power consumption of logic part is 3.88 mW, estimated by using PrimePower^{TM}. The memory blocks are generated by Artisan memory compiler and consume 5.29 mW. The total power consumption is 9.17 mW for the proposed design. When comparing the proposed GICam-II image compressor with GICam-I one in Table 3.6, the power dissipation can further save 38.5% under the approximate condition of quality degradation and compression ratio because of the reduction of memory requirement for G1, G2 and B components.
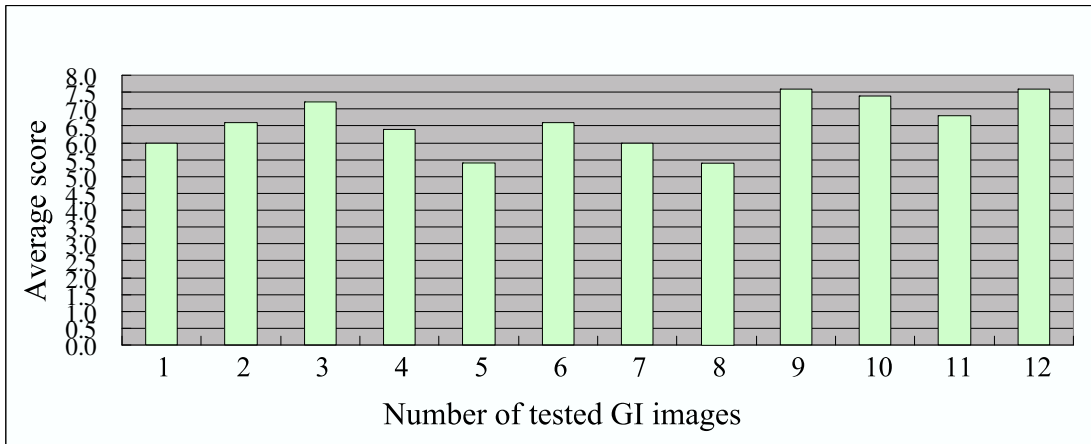
36

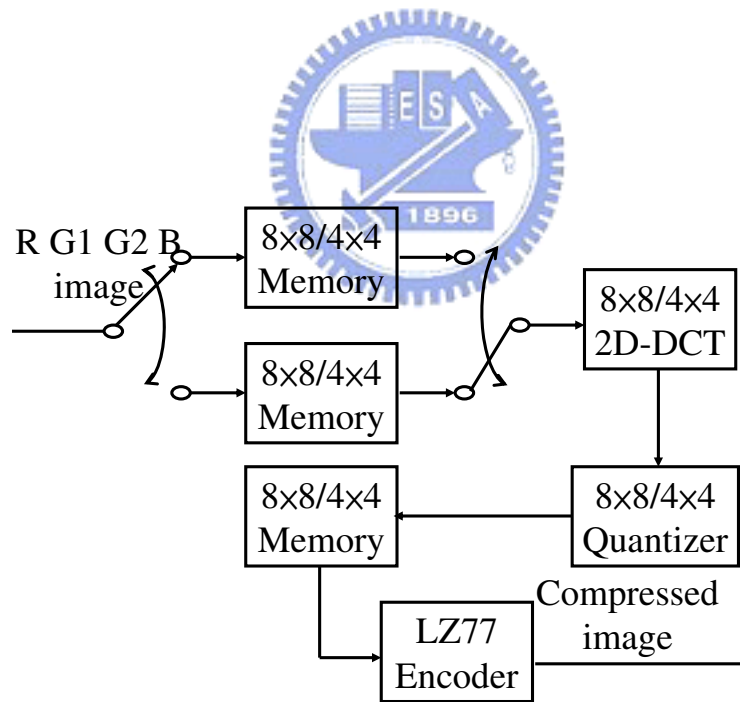Figure 3.18. The evaluation results of professional gastroenterology doctors.

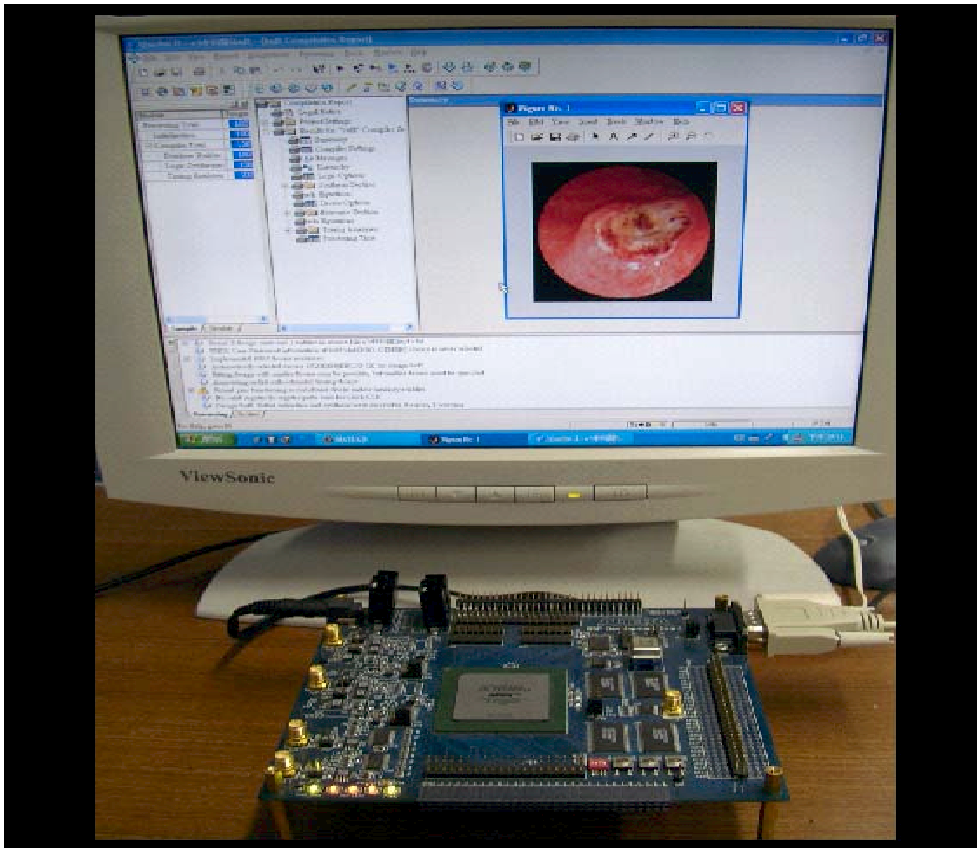Figure 3.19. The GICam-II image compressor.

Figure 3.20. The FPGA prototype of the GICam-II image compressor.

Table 3.6. The comparisons of performance.

Compression algorithm	JPEG	GICam-I image compressor [20]	GICam-II image compressor
Average PSNRY	46.37 dB	41.99 dB	40.73 dB
Average compression rate	82.20%	79.65%	82.28%
Average power dissipation	876 mW	14.92 mW	9.17 mW